JSTT JOURNAL OF SCIENCE AND TRANSPORT TECHNOLOGY

Journal of Science and Transport Technology
Journal homepage: https://jstt.vn/index.php/en

UNIVERSITY OF TRANSPORT TECHNOLOGY

Experimental and GEP-based sensitivity analysis of water and chloride ingress in concrete with varying mix designs and curing conditions

Ho Manh Hung, Huynh Phuong Nam, Pham Van Ngoc, Nguyen Duc Tuan, Phan Hoang Nam*

Faculty of Road and Bridge Engineering, The University of Danang - University of Science and Technology, Danang, Vietnam

Article info
Type of article:
Original research paper

DOI:
https://doi.org/10.58845/jstt.utt.2026.en.6.3.140-160

***Corresponding author:**
Email address:
phnam@dut.udn.vn

Received: 06/10/2025
Received in Revised Form: 02/06/2026
Accepted: 01/08/2026

Abstract: This study presents an experimental and gene expression programming (GEP)-based investigation into concrete resistance to water and chloride ingress under diverse mix designs and curing conditions. A large-scale experimental campaign comprising 250 surface water absorption tests (SWAT) and penetration depth measurements was conducted, covering variations in binder types, water-to-binder ratios, aggregate types, mineral additives, and curing regimes. Water absorption rates were monitored at 2- and 10-minute intervals, followed by systematic assessments of water, chloride penetration depths, and initial absorption rates. Utilizing this dataset, robust GEP models were developed, demonstrating high predictive accuracy for SWAT, penetration depths, and initial water absorption rates. A key novelty of this study is employing GEP for comprehensive sensitivity analysis, revealing the relative influence of each parameter under varied conditions. The analysis identified that while binder types exhibited moderate sensitivity, water-to-binder ratios, mineral additives, aggregate types, and especially curing methods critically governed concrete's resistance to water and chloride ingress. Notably, high-alite cement significantly enhanced water resistance, while slag incorporation effectively reduced chloride ingress, with curing quality remaining a dominant factor in mitigating both. These combined experimental and GEP-driven insights provide valuable guidance for optimizing concrete mix designs and curing practices to improve durability performance under aggressive environmental exposures.

Keywords: Gene expression programming (GEP); surface water absorption test (SWAT); chloride ingress; curing regimes/quality; sensitivity analysis.

1. Introduction

The durability of concrete structures is a paramount concern for civil engineers, particularly in regions exposed to harsh environmental conditions. In areas characterized by high humidity and salt content, aggressive agents can infiltrate concrete structures, hastening the corrosion of steel reinforcements [1]. This challenge is especially pronounced for offshore installations in marine environments [2] and structures located near the coast [3], significantly impacting civil engineering and architectural practices.

Moreover, in regions subject to extreme cold, the detrimental effects of cyclic freezing and thawing are exacerbated by the widespread use of deicing agents during winter, leading to severe scaling and chloride-induced corrosion [4, 5]. The presence of alkalis in these agents can further exacerbate the issue by catalyzing alkali-silica reactions, compromising the structural integrity of concrete elements [6]. These issues have been identified as significant contributors to the deterioration of numerous concrete structures, both onshore and offshore [7, 8].

To enhance concrete durability, the incorporation of mineral additives such as slag and fly ash has proven effective in mitigating chloride ingress [9, 10]. However, it is imperative to underscore the indispensable role of proper curing procedures in realizing the full potential of slag-concrete compositions [11]. Recent research conducted by Otieno et al. [12] employed the chloride conductivity test to assess the impact of chemical composition and slag replacement level on the chloride penetration resistance of concretes. Their findings elucidated a positive correlation between chloride penetration resistance and decreasing water-to-binder ratio (W/B) alongside increasing slag replacement levels. These results underscore the significance of concrete mix design parameters in enhancing the resistance of concrete against chloride ingress, thereby contributing to the broader understanding of concrete durability in chloride-rich environments.

In a study by Yildirim et al. [13], the influence of cement type on concrete's resistance to chloride penetration was examined. Various cement formulations, including two types of granulated blast-furnace slag cement, a sulfate-resisting cement, and a Portland cement blended with fly ash, were subjected to rigorous experimental evaluation. This assessment, conducted through a series of rapid chloride ion penetration tests, revealed that blast-furnace slag cements exhibited the highest resistance against chloride penetration, while pure Portland cement and sulfate-resisting cement demonstrated the lowest resistance.

In a separate investigation, Junior et al. [14] compared different test methods aimed at determining concrete's resistance to chloride penetration. They sought to understand how these methods responded to the presence of fly ash. Their findings indicated that as the fly ash content increased, the measured chloride depths from various tests converged, suggesting a correlation between fly ash content and test outcomes.

Nam and Hosoda [15] undertook surface water absorption tests (SWAT) on nine different mix proportions of slag concretes, examining the effects of various binders, including ordinary Portland cement (OPC), high alite cement (HAC), and ground granulated blast furnace slag (GGBFS). Their investigation aimed to assess the impacts of these binders on the water and chloride penetration resistances of slag concretes. The study concluded that the use of HAC improved the water penetration resistance of slag concretes.

Furthermore, Bao et al. [16] conducted a comprehensive assessment of the durability of cement-based materials incorporating coarse recycled concrete aggregates (RCAs). Through a series of compressive strength, water absorption, salt absorption, and rapid chloride migration tests, they explored the effects of RCA incorporation on material durability. The results indicated that while the inclusion of coarse RCAs generally decreased compressive strength, it concurrently increased water and chloride transport coefficients, suggesting potential implications for material durability.

While the aforementioned studies have made significant strides in evaluating factors such as cement types and coarse aggregates concerning the resistance of concretes to water and chloride penetration, there remains a gap in our understanding regarding the effects of other crucial parameters, such as curing conditions or additives. Furthermore, the majority of these studies have been conducted based on a limited number of tests, potentially leading to deviations in the evaluation of effectiveness.

Despite the valuable insights gained from prior research, there remains a need for a more comprehensive investigation into the impact of various parameters, such as mix designs, curing conditions, and additives, on concrete's resistance to water and chloride penetration. With the emergence of machine learning techniques [17-19], an array of sensitivity analysis methods has become available [20], serving as a pivotal tool for understanding the dynamics of complex systems and identifying influential parameters [21], which are essential for advancing optimization-based design approaches of various material and structural problems [22, 23]. Even though various machine learning techniques have been applied to predict and optimize concrete properties [24-26]; however, a few studies have focused on the water absorption behavior of concrete surfaces. Particularly, Nazari and Riahi [27] applied artificial neural networks (ANN) and gene-expression programming (GEP) for estimating split tensile strength and percentage of water absorption of concretes. The research results illustrated that ANN and GEP algorithms could be used effectively to evaluate the effect of cementitious material on the split tensile strength and percentage water absorption. Recently, Kina et al. [28] applied long short-term memory methodology, support vector regression, and k-nearest neighbors to develop water absorption prediction of fiber-reinforced self-compacting concrete with high accuracy. Szafraniec et al. [29] also used different machine learning algorithms to estimate the water absorption of nanopolymer hydrophobized concrete. More recently, Tipu et al. [30] used various machine learning models to predict surface chloride concentration based on input features related to material composition and environmental conditions. Among these machine learning algorithms, GEP technique is an accurate prediction model with low errors and transparent mathematical equations [27].

In addition, curing regimes and chemical/mineral additives affect durability indicators in a nonlinear and interdependent manner. For instance, inadequate curing may reduce the benefits of SCMs by increasing capillary connectivity, while additive effects may depend on the W/B ratio and moisture conditions. GEP is therefore suitable because it provides explicit nonlinear equations that can capture such coupled effects while retaining interpretability for equation-based sensitivity analysis.

Building on the previous discussions, this study aims to focus on: (i) building a large-scale experimental program comprising 250 SWAT and chloride penetration measurements on concrete samples prepared with varying mix designs and curing conditions, providing a comprehensive dataset for analysis; (ii) developing a machine learning-based sensitivity analysis using GEP, enabling the automatic extraction of transparent predictive models while quantifying the relative influence of input parameters on water and chloride ingress in concrete.

The advance beyond prior GEP applications of the study is demonstrated by (i) establishing a coupled durability dataset that jointly includes surface water absorption kinetics (SWAT at 2 and 10 min), liquid water penetration depth, chloride penetration depth, and the initial water absorption rate, measured under systematically varied binder systems, SCM contents, aggregate types, admixture use, and curing regimes; (ii) using GEP not only as a predictive tool but also as an interpretable, equation-based sensitivity-analysis framework to quantify the influence of each factor across multiple durability indicators; and (iii) explicitly analyzing how curing-regime components (e.g., mould time, water curing, and room curing) interact nonlinearly with mix variables in transparent mathematical forms, thereby providing more actionable insights for durability-oriented mix and curing design.

2. Experimental setup

2.1. Mix proportions

This study investigated the utilization of four distinct types of binders: OPC, HAC, GGBFS, and fly ash (FA). Detailed chemical composition and physical properties of the binders can be found in Table 1, while the clinker-phase composition of the clinker cements (OPC and HAC) is reported in Table 2. In durability interpretation, SCMs influence chloride ingress not only through pore refinement but also through chemical binding mechanisms linked to their oxide composition, particularly alumina-bearing components.

Table 1. Chemical composition and physical properties of binders

Binder	Chemical composition (%)								Density	Specific area
	SiO2	Al2O3	Fe2O3	CaO	MgO	SO3	Na2O	K2O	(g/cm^3)	(cm^2/g)
OPC	20.36	5.33	3.04	64.09	1.50	2.13	0.28	0.36	3.16	3310
HAC	18.76	5.18	2.85	64.16	1.88	3.97	0.42	0.38	3.11	5480
GGBFS	32.30	14.20	0.31	43.40	5.70	1.93	0.26	0.27	2.90	4030
FA	60.2	Loss in ignition (%): 1.5							2.23	3940

Table 2. Bogue phase composition of clinker cements (OPC and HAC)

Cement	Compound composition (%)			
	C3S	C2S	C3A	C4AF
OPC	59.88	13.52	8.99	9.24
HAC	68.36	2.57	8.91	8.66

Table 3. Mix proportions of concretes

Mix proportion	W/B (%)	s/a (%)	Mix compositions (kg/m^3)									
			W	Binder				Sand	Coarse aggregate		Admixture	
				OPC	HAC	Slag	FA		Andesite	Limestone	101	AE
O-40-A	40	45	165	413	-	-	-	750	927	-	1.24	5.0
O-40-S-A				248	-	165	-	745	921	-	1.24	2.1
O-40-F-A				351	-	-	62	740	915	-	2.27	3.7
H-40-S-A				-	248	165	-	744	920	-	1.44	2.5
H-40-F-A				-	351	-	62	739	914	-	2.27	3.7
O-40-S-F-A				210	-	140	62	736	910	-	2.89	1.2
H-40-S-F-A				-	210	140	62	736	910	-	2.89	1.2
O-40-S-L				248	-	165	-	745	-	945	1.24	2.1
O-40-F-L				351	-	-	62	740	-	940	2.68	1.2
H-40-S-L				-	248	165	-	744	-	945	1.24	2.5
H-40-F-L				351	-	-	62	739	-	938	2.68	1.4
O-50-A	50			330	-	-	-	780	965	-	0.99	2.1
O-50-S-A				198	-	132	-	776	960	-	0.99	0.7
O-50-F-A				281	-	-	50	773	955	-	2.15	0.3
H-50-S-A				-	198	132	-	776	959	-	0.99	-
H-50-F-A				-	281	-	50	772	954	-	2.15	-
O-50-S-L				198	-	132	-	776	-	986	0.99	-
O-50-F-L				281	-	-	50	773	-	981	2.15	-
H-50-S-L				-	198	132	-	776	-	985	0.99	-
H-50-F-L				-	281	-	50	772	-	980	2.15	-
O-60-A	60			275	-	-	-	801	990	-	0.83	0.6
O-60-S-A				165	-	111	-	798	986	-	0.83	-
O-60-F-A				234	-	-	41	794	982	-	2.48	-
H-60-S-A				-	165	111	-	797	986	-	1.38	-
H-60-F-A				-	234	-	41	794	982	-	2.75	-

In durability interpretation, SCMs influence chloride ingress through both physical pore refinement and chemical binding mechanisms, which are closely related to their oxide composition. Reactive SCMs such as GGBFS and FA can consume portlandite through pozzolanic or latent hydraulic reactions and generate additional C–S–H or C–A–S–H phases, thereby refining the pore structure, reducing pore connectivity, and limiting ion transport pathways. In addition, alumina-bearing components in SCMs may contribute to the formation of aluminate hydrates, which can enhance chloride binding and reduce the amount of free chloride available for penetration. For slag, the presence of CaO and MgO may further influence reaction kinetics and hydrate assemblage, while the loss on ignition of FA may indicate unburnt carbon, which can affect the interaction with chemical admixtures and, consequently, the fresh and hardened properties of concrete.

The control mix comprised concrete solely composed of OPC. In contrast, various mixes involved partial replacement of cements with slag at ratios of 40%. The W/B ratios spanned from 0.4 to 0.6. Coarse aggregates, sourced from andesite and limestone with a maximum particle size of 19 mm, were employed. To fortify resistance against scaling under freeze/thaw cycles, the air content of the concretes was meticulously controlled at 6% ± 0.5% through the incorporation of an air-entraining agent (AE). Each type of concrete was meticulously prepared with ten cylindrical specimens, boasting a diameter of 100 mm and a height of 200 mm. The precise mix proportions of concrete are detailed in Table 3.

2.2. Sealing, curing conditions, and SWAT

The overall process of the experiment is shown in Figs. 1(a) and (b), corresponding to the SWAT and penetration tests, respectively. Immediately after demolding, the top surface and side of the specimens were sealed, while the bottom remained open to ensure one-directional evaporation or permeation of water, thus allowing for even moisture distribution within the specimen. The sealing process involved wrapping the specimen with alumina tape, followed by coating it with epoxy resin. The epoxy resin required one day for hardening before the curing process continued.

Ten specimens of each type of concrete were subjected to curing for 28 days under five different conditions, ranging from very good to very poor ones, as illustrated in Table 4. Two specimens were prepared for each condition, and the SWAT indices were obtained from both specimens. For the penetration depth test at the age of six weeks, only one specimen was utilized, which was immersed in salt water. The other specimen was reserved for long-term observation at 12 weeks.

For SWAT outputs, two specimens were measured for each mix–curing condition and the mean value was used. For penetration-depth outputs, the six-week destructive test was performed on one specimen per condition; therefore, condition-level standard deviations or confidence intervals cannot be fully reported for these outputs. To reduce measurement uncertainty, the penetration front was measured at multiple points on the split surface and the mean value was used. This limitation is considered when interpreting the data-driven sensitivity results.

Following the curing process, all specimens underwent drying in a room with a temperature of 20°C and relative humidity of 60%. Given that the moisture content of concrete significantly influences its water absorption [31], specimens were dried until their water contents stabilized. According to ASTM-C140-11a [32], stability is achieved when two successive weightings, taken at intervals of 2 hours, show an increase in water loss not exceeding 0.2% of the last previously recorded weight of the specimen. In this study, all specimens reached stability at the age of 63 days.

Before conducting the SWAT, the moisture content of the concrete surface was measured using a moisture tester (HI-520). The initial weight of the specimens was then measured. SWAT, utilizing pure water, was applied to determine the water absorption rates at two minutes and at ten minutes. For cylindrical specimens, a frame was utilized to secure the water cup to the surface of the specimen. Water absorption rates at two minutes and at ten minutes were measured for two specimens of each type of concrete in each curing condition, and the mean value was calculated.

Immediately following the SWAT, specimens were immersed in a 10% NaCl water solution, following the guidelines outlined in JSCE-G572 [33]. Specimens were continuously weighed in accordance with ASTM-C-04 [34] until their weights stabilized. Finally, the specimens were split to measure the penetration depth of liquid water using two methods, and the penetration depth of chloride ions was also measured, as shown in Fig. 1(b).

To measure the penetration depth of liquid water, specimens were split at 42 days after immersion into salt water. Typically, concrete cylindrical specimens are easy to split under minimal pressure, resulting in a flat surface on the split section, facilitating the visual detection of the waterfront. However, due to the epoxy resin coating, a larger load was required for splitting, leading to damage to the concrete near the loaded edges and resulting in a rough surface on the split section. To address this, a high loading rate was employed.

After splitting, the liquid water penetration depth was determined using two complementary approaches (Fig. 1(b)): (1) visual detection of the wet–dry contrast and (2) a color-change indicator. In both approaches, to account for local roughness of the fracture surface and to quantify the associated measurement uncertainty, penetration depth was measured at multiple locations along the waterfront and reported as the mean value:

- Visual detection: The waterfront was observed visually in both halves of the split specimen to detect the color difference between the wet and dry parts. The wet part appeared slightly darker than the dry part. This method provided clearer results in specimens with drier inside parts, such as concrete with low W/B subjected to poor curing.

- Color-change agent: A color-change agent was applied to one half of the specimen to detect the waterfront. This agent, sensitive to the presence of liquid water, was sprayed evenly onto the surface of the section. The waterfront was recorded by marking a zigzag line at the interface between the wet and dry parts. Some points along the front were measured for depth, and the mean value was taken. The results obtained by the color-change agent were consistent with those observed visually.

On the other half of the specimen, the penetration depth of chloride ions was measured by spraying a 0.1mol/l $AgNO_3$ solution onto the surface. The color change from dark to light indicated the presence of chloride ions.

3. Dataset gatherings

Based on experimental analyses, a dataset comprising 250 instances has been compiled, incorporating 15 input variables and 5 output variables. Specifically, the inputs encompass various parameters such as W/B ratio, the quantity in kilogram required for 1m^3 concrete of OPC, HAC, GGBFS, FA, sand, andesite, limestone, super plasticizer 101, AE, curing conditions such as number of days left in the mold after pouring the concrete, number of days curing in water (20^{o}C), number of days curing in the room (20^{o}C, humidity 60%), moisture of sample when testing SWAT at 63 days old (%), number of days soaked in water or soaked in 10% NaCl solution (counted from when the sample was 63 days old). The ranges of the input variables are illustrated in Table 5.

Conversely, the output corresponds to the findings obtained from the SWAT and penetration tests. Specifically, these outputs encompass the SWAT value at 2 minutes measured at age 63 days (ml/m^2/s) (Y_1), the SWAT value at 10 minutes measured at age 63 days (ml/m^2/s) (Y_2), water penetration depth (mm) (Y_3), chloride penetration depth (mm) (Y_4), and initial water absorption rate (mm/$\sqrt{s}$) (Y_5) were the output variables.

Based on the observed dataset, a correlation analysis was conducted among the outputs (Y_1 to Y_5). The results, as shown in Fig. 2, reveal notable relationships among these variables. The correlation between Y_1 and Y_2 is exceptionally high (0.960), reflecting that both indices describe the same surface absorption process at different time scales. Similarly, the correlations between Y_1 and Y_5 (0.822), and Y_2 and Y_5 (0.850) are also notably strong, which is consistent with the role of near-surface capillary absorption in governing early-time uptake. The correlations between Y_1 and water penetration depth Y_3 (0.739) and between Y_2 and Y_3 (0.773) are moderate, indicating that while surface absorption is related to deeper ingress, the relationship is influenced by additional factors such as mixture proportions and curing history.

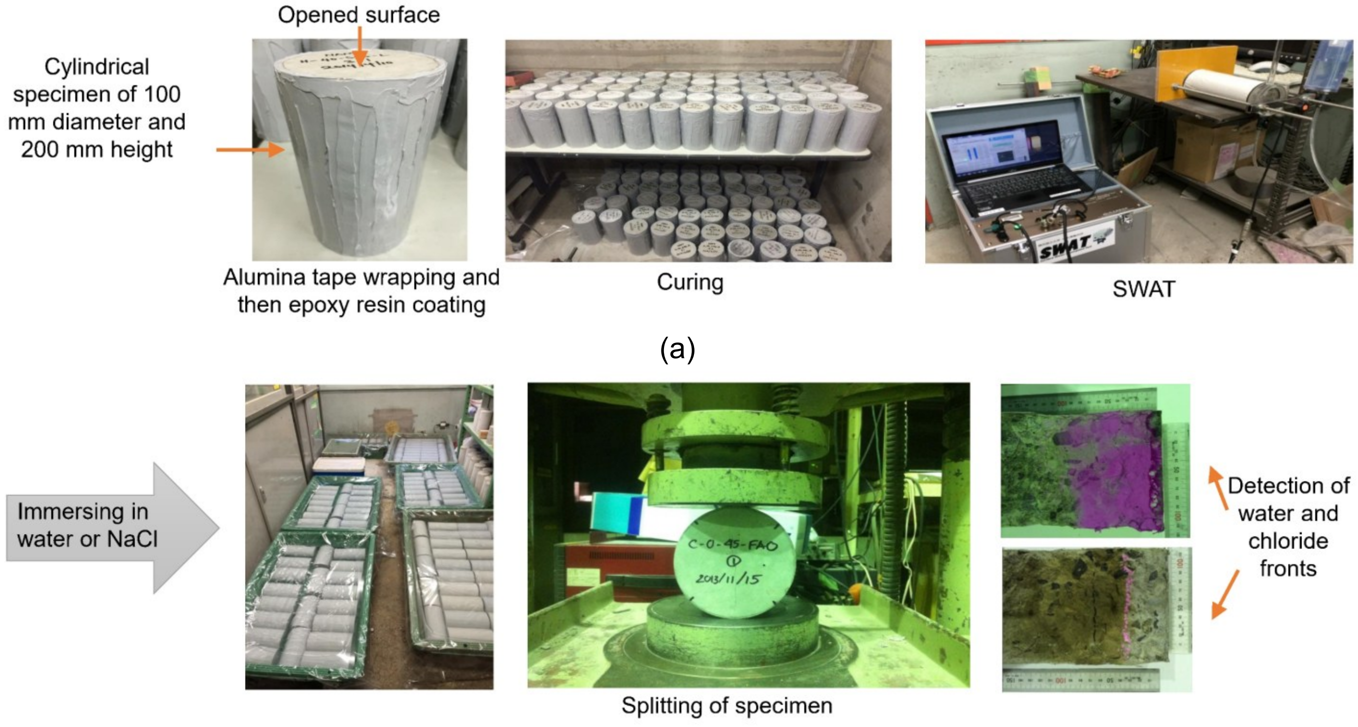

Fig. 1. Experimental setup and process, (a) SWAT test and (b) penetration-depth test

Table 4. Definition of curing regimes

Regime (quality)	Description	Water curing at 20°C (days)	Sealed in curing room 20°C, RH 60% (days)	Unsealed curing room 20°C, RH 60% (days)	NaCl exposure
1 (Very good)	Water curing, then curing room	Day 3–9 → 6	0	Day 9–63 → 54	10% NaCl water from day 63
2 (Good)	Short water curing, then curing room	Day 2–3 → 1	0	Day 3–63 → 60	10% NaCl water from day 63
3 (Moderate)	Sealed in curing room, then curing room	0	Day 1–28 → 27	Day 29–63 → 34	10% NaCl water from day 63
4 (Poor)	Short sealed curing room, then curing room	0	Day 1–8 → 7	Day 8–63 → 55	10% NaCl water from day 63
5 (Very poor)	Curing room only	0	0	Day 2–63 → 61	10% NaCl water from day 63

Notes: Demoulding age varied with the curing regime; demoulding and sealing were completed within one day. NaCl exposure started at day 63.

Table 5. Illustration of input variables

#	Variable	Range	Unit
1	Ratio of water to binder	0.4 - 0.6	
2	Amount of OPC per 1 m^3 concrete	0 - 413	kg
3	Amount of HAC per 1 m^3 concrete	0 - 351	kg
4	Amount of GGBFS per 1 m^3 concrete	0 - 165	kg
5	Amount of FA per 1 m^3 concrete	0 - 62	kg
6	Amount of sand per 1 m^3 concrete	736 - 801	kg
7	Amount of andesite per 1 m^3 concrete	0 - 990	kg
8	Amount of limestone per 1 m^3 concrete	0 - 986	kg
9	Amount of super plasticizer per 1 m^3 concrete	0.83 - 2.89	kg
10	Amount of AE per 1 m^3 concrete	0 - 5	kg
11	Number of days left in the mold after pouring the concrete	1 - 28	day
12	Number of days curing in water (20° C)	0 - 7	day
13	Number of days curing in the room (20° C, humidity 60%)	34 - 61	day
14	Moisture of the sample when testing SWAT at 63 days old (%)	3.5 - 5.2	%
15	Number of days soaked in water or soaked in 10% NaCl solution (counted from when the sample was 63 days old)	42 - 84	day

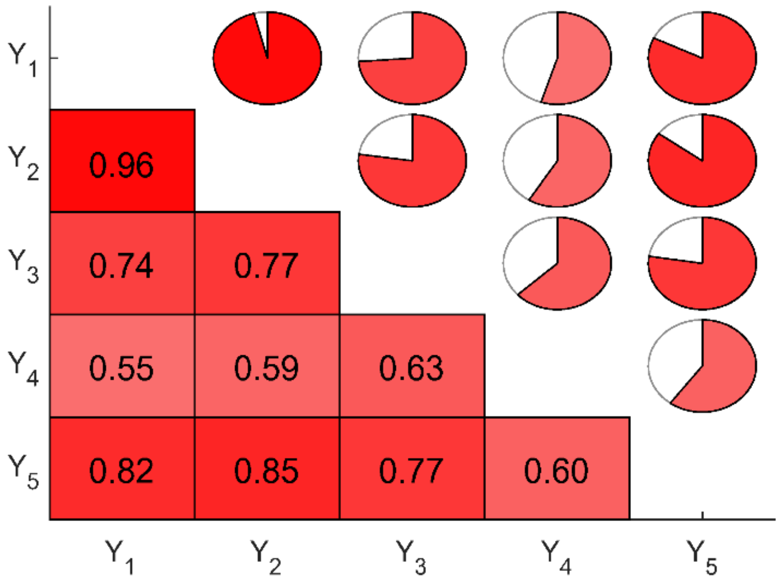

Fig. 2. Correlation analysis between the outputs

Given the very strong Y_1–Y_2 association, Model 2 is retained as an auxiliary conversion relationship expressing Y_2 as a function of Y_1 for practical use when only the 2-minute SWAT result is available. Importantly, this relationship is not used for durability-oriented sensitivity interpretation. Instead, the principal GEP models for Y_1, Y_3, Y_4, and Y_5 use the relevant mix-design and curing variables directly. Overall, the correlation analysis provides useful context for interpreting the measured outputs and supports an optional SWAT time-scaling relationship, while confirming that water absorption, water penetration, chloride penetration, and initial absorption require multivariable models incorporating mixture and curing parameters.

4. GEP model development and validation

GEP is a machine learning approach inspired by Darwinian principles of evolution, utilized to tackle scientific challenges by representing solutions through expression trees composed of genes and chromosomes. GEP evolves through processes such as selection, mutation, transposition, and crossover to develop subsequent iterations [35]. Pham et al. [36] demonstrated GEP's effectiveness and reliability. For a comprehensive understanding of the GEP algorithm, studies by Nguyen et al. [37], and Alaskar et al. [38] offer detailed insights. In this study, GEP models for estimating water and chlorine absorption were developed using GeneXpro Tools 5.0 software.

Multiple GEP trial runs were conducted for each output using the full set of 15 candidate inputs listed in Table 5. Across the best-performing solutions, the evolved expressions consistently retained 12 variables, while the remaining three variables showed negligible contribution and therefore did not appear in the final models. In this study, this behavior is treated as an outcome of the evolutionary search (not a manual feature-elimination step), and the final models were selected to ensure high accuracy and stable generalization for subsequent sensitivity analysis. Consequently, the input variables were optimized, encompassing 9 mix design parameters (W/B, the amount of OPC, HAC, GGBFS, FA, andesite, limestone, super plasticizer, AE per 1 m^3 concrete) and 3 curing conditions (number of days left in the mold after pouring the concrete, curing in water, and curing in the room). This automatic feature selection capability of GEP is a key advantage, enabling the identification of relevant features and interactions during the evolutionary process, thereby reducing the necessity for manual feature engineering and potentially enhancing model performance.

Moreover, critical components essential for deriving solutions include the function set, terminal set, fitness function, control variables, and termination condition [36]. The developed models comprised one to nine genes (sub-expression trees), 30-300 chromosomes, and a head size of 7-12. Sub-expression trees were linked using the addition operator (+), and the fitness function employed was root mean square error (RMSE). Sixteen different mathematical operators were utilized (refer to Table 6), with specific parameter settings detailed in Table 7. For validation purposes, the dataset was partitioned into training and testing based on a k-fold partitioning process, allocating 70% (175 points) for model development (training subset) and 30% (75 points) for model evaluation (testing subset).

Table 6. Function selection for the GEP modeling

Name	Representation	Arity	Definition
Addition	+	2	(x+y)
Subtraction	_	2	(x-y)
Multiplication	*	2	(xy)
Power	Pow	2	pow(x,y)
Square root	Sqrt	1	sqrt(x)
Exponential	Exp	1	exp(x)
Natural logarithm	Ln	1	In(x)
Inverse	Inv	1	1/x
x to the power of 2	X2	1	x^2
x to the power of 3	X3	1	x^3
x to the power of 4	X4	1	x^4
Cube root	3Rt	1	x^(1/3)
Addition with 4 inputs	Add4	4	(a+b+c+d)
Subtraction with 4 inputs	Sub4	4	(a-b-c-d)
Multiplication with 4 inputs	Mul4	4	(a*b*c*d)
Minimum of 2 inputs	Min2	2	min(x,y)

Table 7. Parameter setting for the GEP modeling

Parameter	Model 1	Model 2	Model 3	Model 4	Model 5
Chromosomes	250	30	200	200	300
Genes	9	1	9	9	9
Head size	10	7	12	10	10
Tail size	31	22	37	31	31
Gene size	72	51	86	72	72
Linking function	Addition	Addition	Addition	Addition	Addition
Function	RMSE	RMSE	RMSE	RMSE	RMSE

Based on the optimized parameters above, five different GEP models are developed as the following:

Model 1: SWAT value at 2 minutes measured at age 63 days (ml/m^2/s) described by all the inputs $\widehat{Y}_1$

Model 2: Auxiliary conversion model between SWAT at 2 min and 10 min $\widehat{Y}_2$

Model 3: Water penetration depth (mm) described by all the inputs $\widehat{Y}_3$

Model 4: Chloride penetration depth (mm) described by all the inputs $\widehat{Y}_4$

Model 5: Initial water absorption rate Si (mm/$\sqrt{s}$) described by all the inputs $\widehat{Y}_5$

$$\begin{aligned}\widehat{Y}_1=&\left[(d_8-d_6-d_5(d_{10}+d_8)-d_9-d_7-0.34)^2-d_7^2\right]^{-1}+\exp\left(-1.86-(2d_0)^{d_8d_{11}}-(d_4+d_5)(d_2d_8d_{10}d_{11})\right)-e^{-4.5}+d_0-0.35\\&+\left[\left(d_6^{1/3}\cdot d_1\cdot d_3^2\cdot(-5.79)-d_9+2.34\right)^2-d_0^{-1}\right]^{-1}+(d_8-d_5-d_3-6.41)^{-2}\\&+2.74\cdot(-0.65d_1+d_9+d_6-21.98+2d_{11})^{-1}+\left(d_9+5.10-d_7^{-10.41}+531.62d_{10}d_0\right)^{-2/3}\end{aligned} \tag{1}$$

$$\widehat{Y}_2=\widehat{Y}_1\cdot\ln(10.74-2\widehat{Y_1}) \tag{2}$$

$$\begin{aligned}\widehat{Y}_3=&\left[d_{10}-d_2-d_6+d_8(1-1.930d_8^2)-d_9+0.940\right]^{-1}+(1-d_{10})+\exp\left(6.066-(-0.232d_{10}d_{11}+d_5)^2-d_9-e^{d_7+d_9}\right)\\&+\ln\left(1-[11.25d_0d_{10}-1.526+d_9]^{-3}\right)+(d_0-0.511)^{-1/9}+\left[d_0-d_0^{3d_9}+0.0253d_3d_4d_9-3.139d_2d_3d_5^2d_{11}\right]^{-1}+9.749\\&+\left[d_{10}-d_9-(6.771-d_{10}+d_1+d_3)^{-1}-4.922^{-1/2}\right]^{1/3}-\ln d_7+\exp\left(d_0\cdot\exp\left((1.349-d_0-d_5+d_{10}^2)^{-1}\right)\right)-\sqrt{2d_8}\end{aligned} \tag{3}$$

$$\begin{aligned}\widehat{Y}_4=&\left(\left(d_0d_1d_4d_9+d_9^{-1}+8.430-d_7\right)^{1/2}-d_3^{0.5d_0}\right)^{-1}+\ln\left(e^{3d_0}-\left(1-\frac{1}{2}\ln d_9\right)\right)+7.768\\&+\left(9.520e^{d_{10}}-2d_{10}-8.443-d_9\right)^{-2/3}+(d_1+d_8+d_9)^{-\frac{1}{3}(d_5+0.33)}-(\ln(d_0+d_3+0.224))^{-1}\\&+\left((-1.411d_0^2d_{10})^3+2d_2+d_8+d_9+2d_{10}+d_6-0.832\right)^{-1}+\left(d_0+\left(d_4^{d_{11}}+1.079\right)^{-d_8}\right)^3\end{aligned} \tag{4}$$

$$\begin{aligned}\widehat{Y}_5=&d_9^{-1}+\exp\left[\left(-3.62\cdot d_9^{-1}\cdot\left(\frac{1}{4.03}+d_8\right)\cdot\min(d_{10},1.23)\right)^9\right]+\min\left(d_5,d_9^{-1/3}\right)\\&+\exp\left[\min\left(-3.50,\left(-7.03+(d_8+d_2)^3\right)^3\right)\right]-2.68+\min\left(d_0^{1/3e^{d_{10}}\cdot 0.56^3\cdot d_3^{d_4}\cdot d_9},d_1\right)\\&+\min\left((d_9-4.39-d_{10}-1.3\cdot 10^{-5})^2,d_9^{1/3}\right)^{-1}+\left[\exp\left(d_4-\min(d_6,d_7)\cdot 8.05^{-1}\right)^{1/3}\right]^{-2/3}\\&+\exp\left[\left(\min\left((-2.07\cdot d_0)^{d_{11}},-0.66\right)\right)^{-1/3}+d_9^{-1}\right]+d_7\left((d_1+d_{11}-33.27)^{1/3e^{0.87\cdot d_{10}}}\right)\end{aligned} \tag{5}$$

Notes: d_0: W/B ratio; d_1: OPC amount (kg); d_2: HAC amount (kg); d_3: GGBFS amount (kg); d_4: FA amount (kg); d_5: Andesite amount (kg); d_6: Limestone amount (kg); d_7: Super plasticizer amount (kg); d_8: AE amount (kg); d_9: Number of days left in the mold after pouring the concrete (day); d_{10}: Number of days curing water at 20^o (day); d_{11}: Number of days curing in the room (20^o, humidity 60%) (day).

In the GEP formulations, curing-component variables are included explicitly and are allowed to interact with mixture-proportion variables during model evolution, so that coupled nonlinear effects can be captured in the resulting analytical expressions.

Because GEP is stochastic, different runs may lead to algebraically different but similarly performing expressions. Therefore, the final equations are used as interpretable predictive models within the tested domain, while the sensitivity discussion emphasizes stable variable groups and trends rather than claiming uniqueness of one symbolic expression

Fig. 3 illustrates the regression plots depicting the performance of the five models during both training and testing phases, along with comparative analyses shown in Table 8. Notably, all models exhibit consistently high correlation coefficients (R-values) ranging from 0.878 to 0.968, translating to R^2 values between 0.771 and 0.937. Additionally, the RMSE and mean absolute error (MAE) values for these models are notably low and within acceptable limits. For instance, Model 1 demonstrates an RMSE of 0.072 ml/m2/s and an MAE of 0.057 ml/m2/s, further affirming the reliability of the proposed GEP-based models.

The proposed GEP equations are intended for interpolation and sensitivity interpretation within the experimental domain covered by the 250 observations; extrapolation to binders, aggregate systems, curing histories, or W/B ranges outside those listed in Table 5 should be performed with caution and preferably supported by additional validation data.

Table 8. Performance of the proposed GEP-based models 1-5

	Model 1		Model 2		Model 3		Model 4		Model 5	
Phase	Training	Test	Training	Test	Training	Test	Training	Test	Training	Test
R^2	0.874	0.887	0.919	0.937	0.771	0.786	0.791	0.779	0.887	0.868
R-value	0.935	0.942	0.959	0.968	0.878	0.887	0.889	0.883	0.942	0.932
RMSE	0.072	0.071	0.028	0.026	3.532	2.321	2.463	2.127	0.668	0.718
MAE	0.057	0.054	0.022	0.021	2.536	1.585	1.898	1.717	0.503	0.549

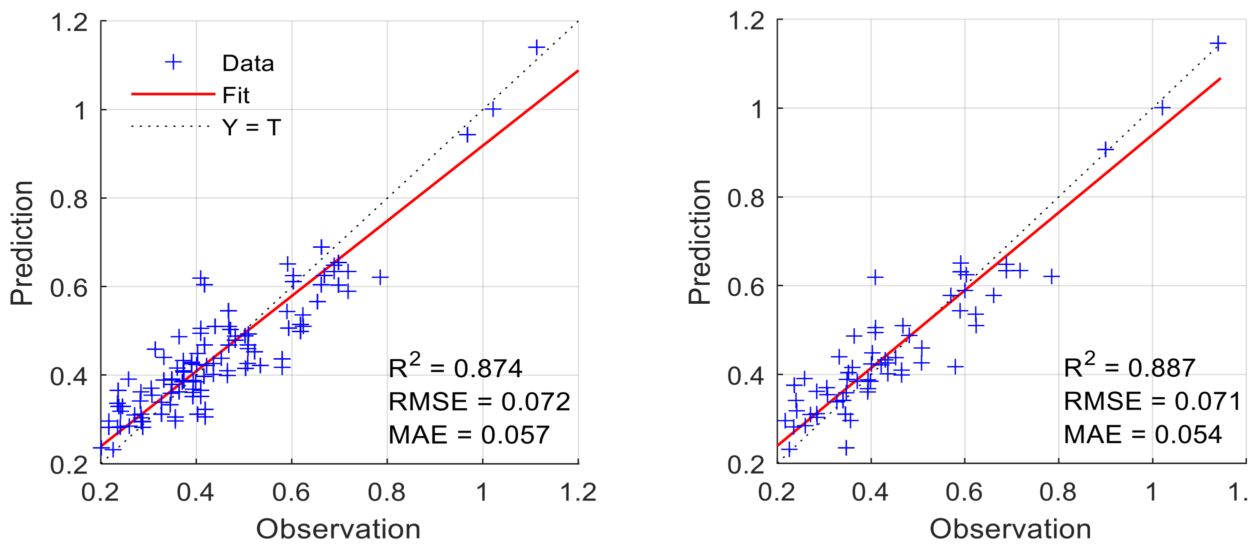

(a)

Fig. 3. Regression plots of the training set (left) and test set (right) for (a) Model 1, (b) Model 2, (c) Model 3, (d) Model 4, and (e) Model 5

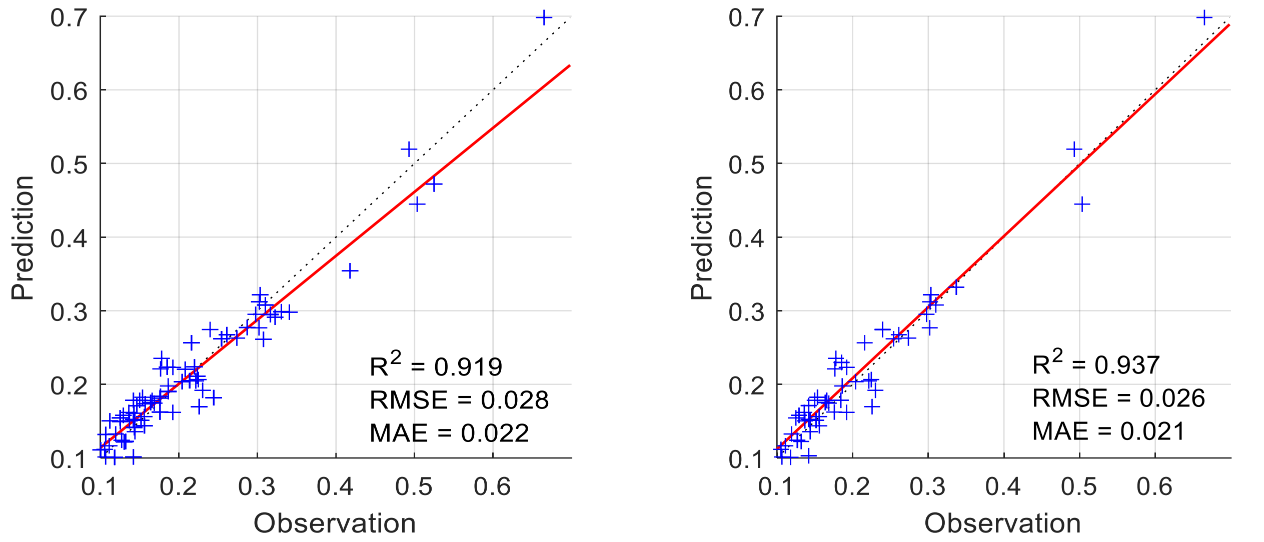

(b)

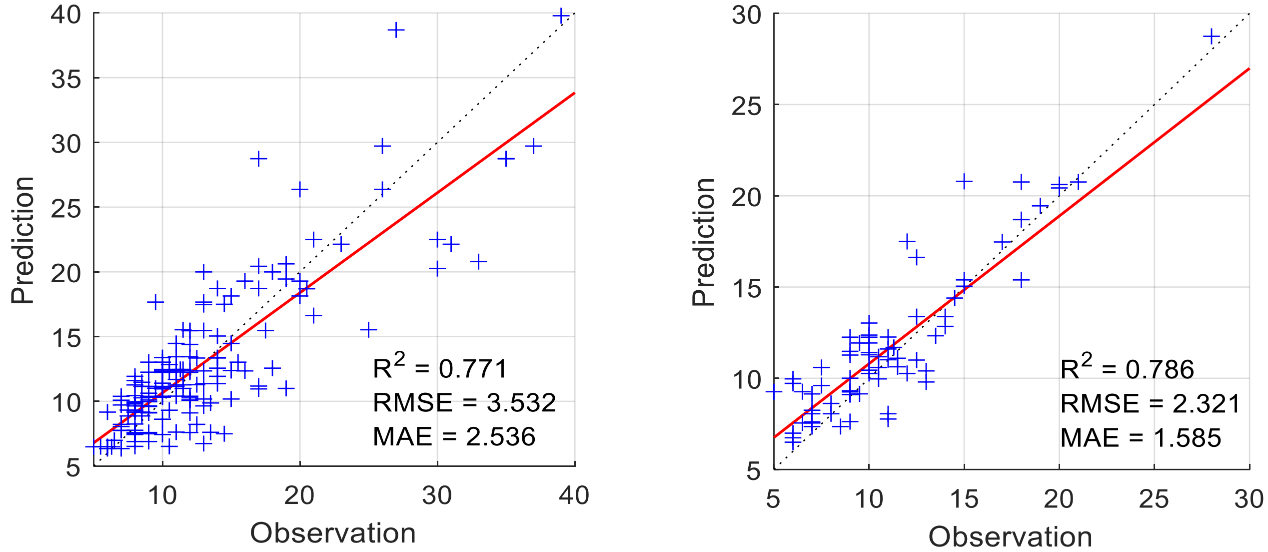

(c)

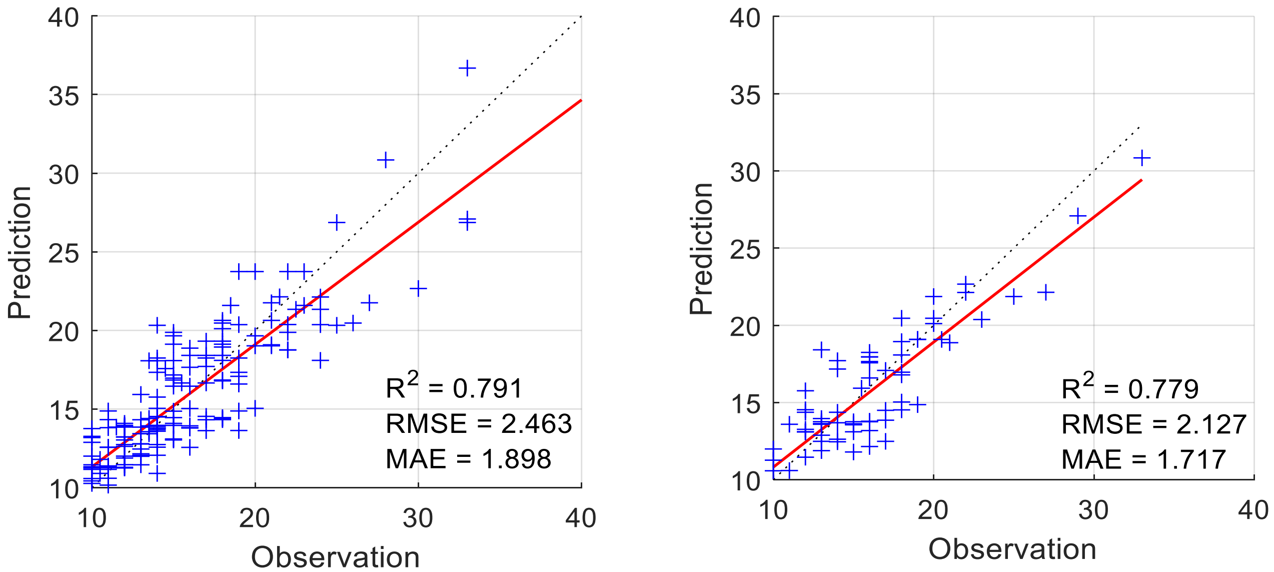

(d)

Fig. 3. (continued)

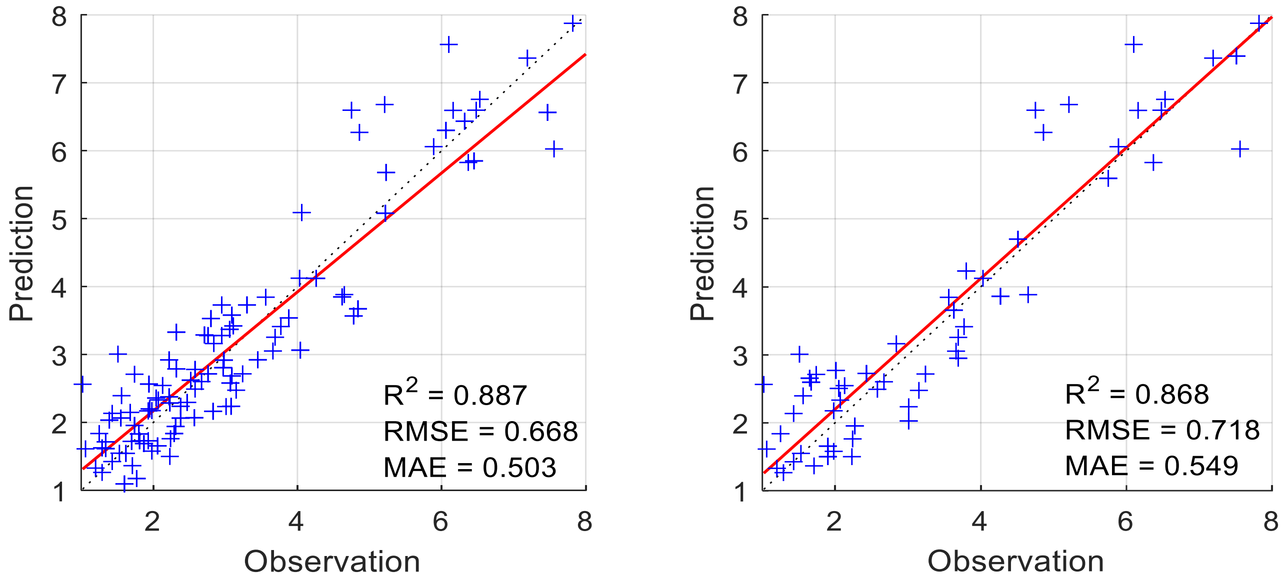

(e)

Fig. 3. (continued)

5. Sensitivity analysis

The sensitivity analyses conducted on the obtained GEP models provide valuable insights into the determinants influencing the SWAT results at 2 minutes and the depths of water and chlorine absorption. These analyses are calculated by considering the effect of each input variable, while other ones are set by their mean values [39]. The sensitivity score (SC) can be obtained as follows,

$$N_i = Y_{max}(\mathbf{x}_i) - Y_{min}(\mathbf{x}_i),$$

$$SC = \frac{N_i}{\sum_{i=1}^{n} N_i}, \qquad (6)$$

where $Y_{max}(\mathbf{x}_i)$ and $Y_{min}(\mathbf{x}_i)$ are the maximum and minimum of the predicted responses for the i^{th} input variable.

The sensitivity score used here is a one-variable-at-a-time, equation-based index. It is therefore conditional on the mean values assigned to the remaining variables and on the tested input ranges. The rankings should be interpreted as practical sensitivity indicators within the present experimental domain, not as a full global sensitivity or causal decomposition of all interaction effects.

Although the GEP equations can represent nonlinear and interaction-like terms among input variables; the sensitivity index used in this study provides first-order conditional rankings by varying one input at a time. Thus, interaction mechanisms are discussed qualitatively based on the nonlinear GEP expressions and concrete durability literature, while quantitative decomposition of interaction effects is beyond the scope of this study.

Because several input variables are compositionally or procedurally related, the sensitivity rankings should be interpreted as conditional, equation-based importance measures within the experimental design, rather than as fully independent causal effects. In particular, binder/SCM variables and curing-duration variables may partly reflect correlated design choices; therefore, their rankings are discussed together with their physical context and tested ranges

5.1. Sensitivity to SWAT results

The sensitivity analysis for SWAT at 2 minutes (Model 1) is presented in Fig. 4, and the corresponding numerical ranking is summarized in Table 9. The ranking table quantifies the relative influence of each input on early-time surface water absorption, where a higher sensitivity score indicates a stronger contribution to the predicted SWAT response.

As shown in Table 9, andesite aggregate (d_5) is the most influential factor (importance 22.15%), followed by the curing components water curing (d_{10}, 18.58%), room curing (d_{11}, 17.35%), and mold curing (d_9, 16.67%). Together, these four variables account for approximately 74.75% of the total sensitivity, highlighting that early-time absorption is governed primarily by near-surface transport conditions shaped by aggregate-related surface/ITZ effects and early-age curing quality. The next most influential factor is limestone (d_6, 11.85%), while W/B (d_0) shows a moderate contribution (4.11%) in the present dataset.

W/B (d_0, 4.11%) exhibits moderate sensitivity. Physically, increasing W/B generally increases capillary porosity and pore connectivity because a larger fraction of mixing water is not consumed during hydration, which can enhance early-time sorptivity. Conversely, lower W/B promotes a denser microstructure and reduces connectivity of capillary pores, limiting water uptake. However, the sensitivity ranking indicates that for a short-duration (2-min) surface absorption index, the effective transport network near the exposed surface can be governed more strongly by aggregate/ITZ characteristics and curing-controlled surface densification than by the discrete W/B variation (0.40–0.60) alone.

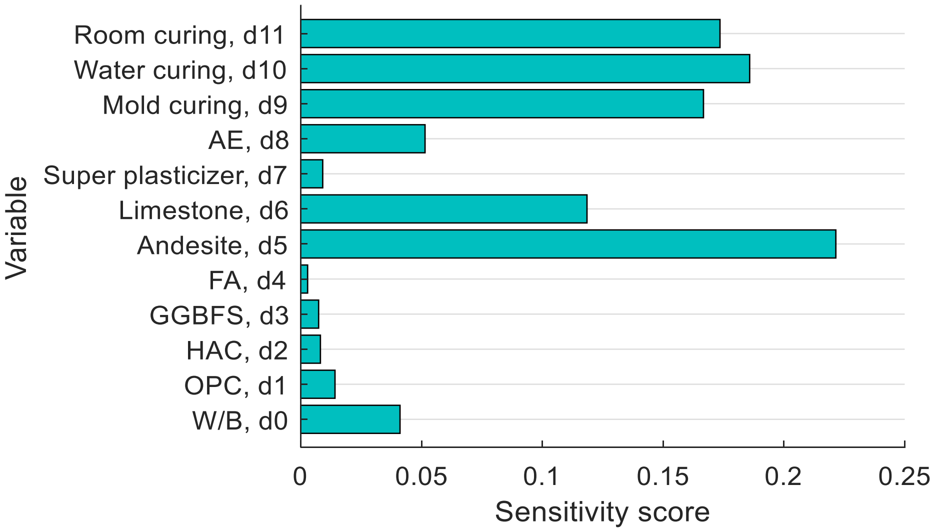

Fig. 4. Sensitivity analysis result to SWAT at 2 minutes after 63 days

Table 9. Sensitivity ranking for the 2-minute-SWAT model (Model 1)

Rank	Variable	Variable Importance	Importance (%)	Cumulative (%)
1	d_5	0.2215	22.15	22.15
2	d_{10}	0.1858	18.58	40.73
3	d_{11}	0.1735	17.35	58.08
4	d_9	0.1657	16.67	74.75
5	d_6	0.1185	11.85	86.60
6	d_8	0.0514	5.14	91.74
7	d_0	0.0411	4.11	95.85
8	d_1	0.0142	1.42	97.26
9	d_7	0.0091	0.91	98.17
10	d_2	0.0081	0.81	98.98
11	d_3	0.0074	0.74	99.72
12	d_4	0.0028	0.28	100.00

Binder type and cement chemistry (d_1–d_2) show relatively low sensitivity for SWAT at 2 minutes (OPC d_1: 1.42%; HAC d_2: 0.81%). Although HAC may accelerate hydration and promote rapid pore refinement, its influence on the 2-min surface absorption response is comparatively smaller than curing and aggregate effects. This suggests that, for very early-time SWAT, the controlling mechanism is not only binder chemistry but also the formation quality of the near-surface zone, which is strongly affected by curing history.

SCMs (GGBFS d_3 and FA d_4) have low sensitivity for this output (0.74% and 0.28%, respectively). This is consistent with the fact that SCM contributions to pore refinement and transport resistance are often more pronounced at later ages, while the 2-minute SWAT response is dominated by surface-zone connectivity and moisture condition. Nevertheless, SCMs can still contribute indirectly by improving later-age densification and reducing permeability, but their direct influence on the 2-minute SWAT sensitivity is limited in the present dataset.

Aggregate effects dominate the SWAT response. The high importance of andesite (d_5, 22.15%) and limestone (d_6, 11.85%) indicates that coarse aggregate type can substantially influence early-time (2-min) surface water absorption. This is physically plausible because SWAT at 2 minutes primarily probes transport in the near-surface zone, where aggregate-related characteristics (e.g., surface texture/roughness, intrinsic absorption, and mineralogy) and the resulting interfacial transition zone (ITZ) can strongly affect local connectivity and preferential flow paths. The ITZ is widely recognized as a comparatively more porous region than the bulk paste and can act as a preferential pathway for fluid transport; its microstructure depends on aggregate surface characteristics and paste–aggregate bonding [40]. Consequently, a change in aggregate system (andesite versus limestone) can induce a stronger sensitivity signal than the discrete W/B variation considered in this dataset, particularly for a short-duration surface absorption index. In this sense, the observed ranking does not contradict the role of w/b, but rather highlights that, for 2-minute SWAT, aggregate/ITZ-related effects and curing-controlled surface densification can dominate within the investigated experimental domain [41].

The air-entraining agent (AE, d_8) shows a non-negligible contribution (5.14%), consistent with its role in introducing distributed air voids that can interrupt capillary continuity and reduce sorptive transport in the paste and near-surface region (while also improving freeze–thaw resistance). The superplasticizer (d_7) has a small direct sensitivity (0.91%), which is reasonable because its primary benefit for transport resistance is often indirect, enabling lower W/B at a given workability and improving compaction, rather than directly altering transport at a fixed mixture composition.

The curing components d_9–d_{11} collectively account for 52.60% of the total sensitivity (Table 9), confirming that curing quality is one of the most critical determinants of SWAT. Adequate curing reduces moisture loss and supports sustained hydration, leading to higher degrees of hydration, refined pore structure, and reduced near-surface connectivity. Water curing (d_{10}) ranks highest among curing parameters, consistent with its effectiveness in maintaining saturation and promoting continued hydration. Mold curing (d_9) and room curing (d_{11}) also show strong influence because they shape early-age moisture gradients and surface densification, which directly affect early-time absorption.

5.2. Sensitivity to the penetration depth of water and chloride

The GEP-based sensitivity analyses for water penetration depth (Model 3) and chloride penetration depth (Model 4) are shown in Fig 5 and Fig 6, respectively. The corresponding numerical rankings are summarized in Table 10 and Table 11, which report the sensitivity importance, percentage contribution, and cumulative contribution of each variable. Overall, both outputs are dominated by curing-related variables, but the material drivers differ between water ingress and chloride ingress, reflecting different governing mechanisms.

(a) Water penetration depth (Model 3)

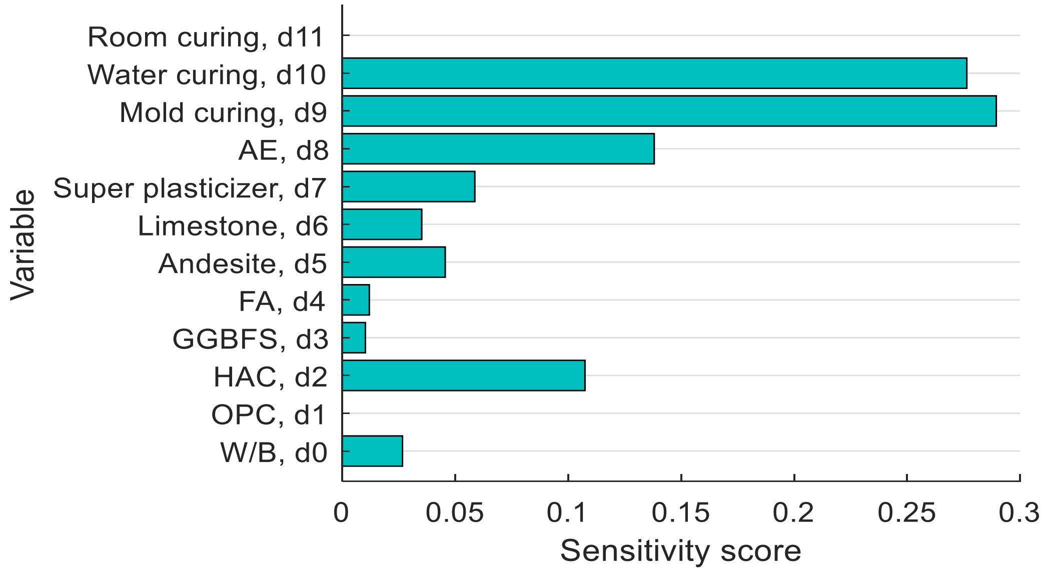

Fig. 5. Sensitivity analysis results for water penetration depth

Table 10. Sensitivity ranking for the water penetration depth model (Model 3)

Rank	Variable	Variable Importance	Importance (%)	Cumulative (%)
1	d_9	0.2894	28.94	28.94
2	d_{10}	0.2764	27.64	56.58
3	d_8	0.1381	13.81	70.38
4	d_2	0.1075	10.75	81.13
5	d_7	0.0587	5.87	87.00
6	d_5	0.0456	4.56	91.56
7	d_6	0.0352	3.52	95.08
8	d_0	0.0267	2.67	97.75
9	d_4	0.0120	1.20	98.95
10	d_3	0.0103	1.03	99.98
11	d_1	~0.0001	~0.01	99.99
12	d_{11}	~0.0001	~0.01	100.00

For water penetration depth (Fig 5 and Table 10), the sensitivity ranking is strongly governed by curing components: mold curing (d_9, 28.94%) and water curing (d_{10}, 27.64%) together account for 56.58% of the total sensitivity. This indicates that sustained early-age curing is the primary determinant of resistance to liquid water ingress, consistent with its role in promoting continued hydration and pore refinement. The next most influential factor is AE (d_8, 13.81%), followed by HAC (d_2, 10.75%), so the top four variables cumulatively explain 81.13% of the sensitivity. Mechanistically, AE can disrupt capillary continuity through a stable air-void system, reducing sorptive transport and penetration pathways, while HAC can accelerate early hydration and densify the matrix, thus lowering permeability and water penetration.

In contrast, the W/B variable (d_0) shows low-to-moderate influence for water penetration depth (2.67%), and SCM variables such as GGBFS (d_3, 1.03%) and FA (d_4, 1.20%) contribute relatively little to this output within the investigated age and curing domain. Aggregate-related variables also have smaller contributions (andesite d_5: 4.56%; limestone d_6: 3.52%), suggesting that for deeper water penetration, the dominant control is the degree of hydration and near-continuous pore refinement achieved through curing rather than mixture parameters alone.

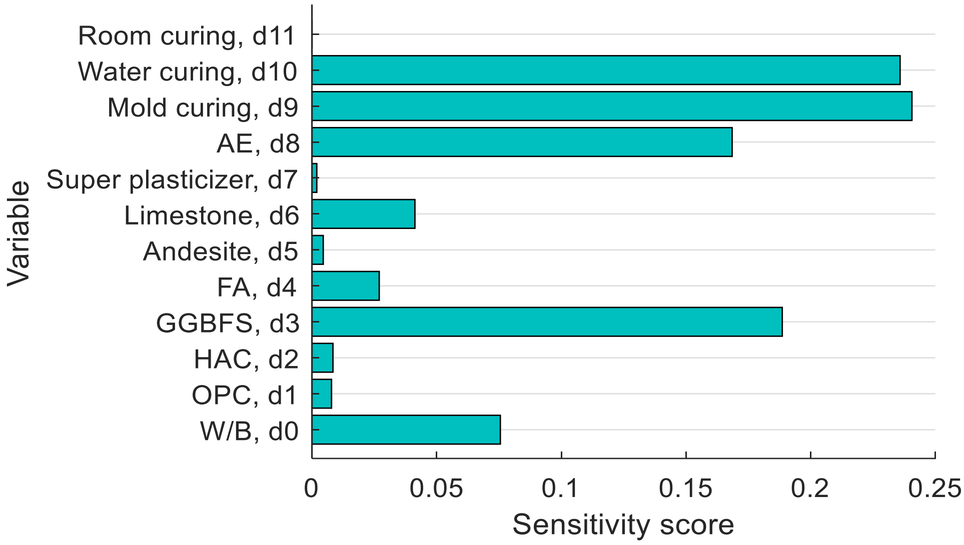

Fig. 6. Sensitivity analysis results for chloride penetration depth

Table 11. Sensitivity ranking for the chloride penetration depth model (Model 4)

Rank	Variable	Variable Importance	Importance (%)	Cumulative (%)
1	d_9	0.2406	24.06	24.06
2	d_{10}	0.2359	23.59	47.65
3	d_3	0.1886	18.86	66.51
4	d_8	0.1685	16.85	83.36
5	d_0	0.0755	7.55	90.91
6	d_6	0.0413	4.13	95.03
7	d_4	0.0270	2.70	97.73
8	d_2	0.0084	0.84	98.57
9	d_1	0.0078	0.78	99.35
10	d_5	0.0045	0.45	99.80
11	d_7	0.0019	0.19	99.99
12	d_{11}	~0.0001	~0.01	100.00

(b) Chloride penetration depth (Model 4)

For chloride penetration depth (Fig. 6 and Table 11), curing remains the leading driver: d_9 (24.06%) and d_{10} (23.59%) contribute a combined 47.65%, confirming that curing quality strongly conditions chloride resistance by controlling pore structure development and connectivity. Importantly, Table 11 provides a quantitative basis to separate the roles of pore connectivity (W/B) and SCM-related effects (GGBFS), as requested by Reviewer 2. Using the variable mapping ($d_0 \rightarrow$ W/B, $d_3 \rightarrow$ GGBFS content), the sensitivity importance of GGBFS (d_3) is 0.1886 (18.86%), while the sensitivity importance of W/B (d_0) is 0.0755 (7.55%). Thus, in this dataset, the contribution of GGBFS to chloride penetration sensitivity is approximately 2.5× that of W/B, indicating that SCM-related mechanisms (pore refinement and chloride-binding-related effects) play a stronger role than W/B alone for chloride ingress under the tested conditions.

Additionally, AE (d_8) ranks highly for chloride penetration (16.85%), which is consistent with the air-void system interrupting capillary continuity and reducing effective transport pathways. After curing, GGBFS, and AE, the remaining variables contribute comparatively less (e.g., limestone d_6: 4.13%, FA d_4: 2.70%, and others below 1%). This ranked structure supports a mechanistic interpretation: chloride ingress is governed by a combination of (i) curing-controlled pore development, (ii) SCM-related refinement/binding effects captured by GGBFS, and (iii) transport-path disruption due to AE, while W/B remains a secondary but non-negligible contributor through pore connectivity and tortuosity.

Taken together, the results show that curing components (d_9–d_{10}) are the dominant controls for both water and chloride penetration. For water penetration, AE and HAC emerge as important secondary drivers (Table 10), whereas for chloride penetration, GGBFS and AE are the key secondary drivers, and W/B plays a smaller but measurable role (Table 11). These results emphasize that improving ingress resistance in aggressive environments requires prioritizing adequate early curing, and for chloride-exposed applications specifically, combining good curing with GGBFS incorporation and appropriate air-void control provides a stronger benefit than W/B adjustment alone within the studied parameter range.

The mechanistic explanations proposed in this section should be regarded as physically plausible interpretations of the GEP-based statistical trends, supported by existing durability literature, rather than direct microstructural proof from the present experiments. Direct verification of ITZ morphology, pore-size distribution, and chloride binding would require additional microstructural/chemical testing and is recommended for future work.

6. Conclusions

This study combined a large experimental program (250 specimens) with GEP to model surface water absorption and water/chloride penetration of concrete across varied binder systems, admixtures, aggregate types, W/B ratios (0.40–0.60), and curing regimes. The main conclusions and practical implications are:

Correlation analyses indicated that the 2-minute and 10-minute SWAT showed an exceptionally high correlation, indicating that the 2-minute SWAT can serve as a rapid screening index for surface absorption performance when time or testing resources are limited. The moderate correlations between SWAT and penetration depths confirm that surface absorption and deeper water/chloride ingress are related but not equivalent; therefore, mix design and curing must be evaluated using multiple durability indicators, not SWAT alone.

The GEP models achieved high accuracy (R = 0.878–0.968; R^2 = 0.771–0.937, with low RMSE/MAE), demonstrating that GEP is effective for capturing nonlinear durability behavior and for extracting interpretable relationships suitable for sensitivity-based interpretation.

Design priorities from the sensitivity ranking are as follows:

Ensuring adequate early curing (mould/water curing components) provides the largest improvement in resistance to water and chloride ingress. Practically, prioritize extending early moist curing in chloride-exposed applications.

Higher W/B increases pore connectivity and consistently worsens ingress resistance; therefore, limit W/B to the lowest feasible level consistent with workability and compaction.

GGBFS shows moderate-to-high influence on chloride penetration, supporting its use to enhance long-term chloride resistance; FA shows smaller but positive long-term effects.

HAC exhibits a strong influence on water ingress resistance, suggesting it as a practical option where reduced capillary suction is critical.

Air entrainment and superplasticizer use contribute to reduced transport (directly by interrupting capillary continuity and indirectly by enabling lower W/B), while aggregate type affects near-surface absorption and ITZ-related transport.

Acknowledgments

This work was supported by The University of Danang – University of Science and Technology, Project code number T2025-02-13.

Data Availability

The dataset used in this study is openly available data with a DOI 10.17632/7tsdtx8x5s.1.

Declaration of Generative AI

During the preparation of this work, the authors do not use Generative AI and AI-assisted technologies tools in order to generate the content of the manuscript.

References

[1]. L.F. Yang, R. Cai, B. Yu. (2017). Investigation of computational model for surface chloride concentration of concrete in marine atmosphere zone. *Ocean Engineering*, 138, 105-111. https://doi.org/10.1016/j.oceaneng.2017.04.024

[2]. R.P. Fernández, M.L. Pardo. (2013). Offshore concrete structures. *Ocean Engineering*, 58, 304-316. https://doi.org/10.1016/j.oceaneng.2012.11.007

[3]. R. Qian, Q. Li, C. Fu, Y. Zhang, Y. Wang, X. Jin. (2023). Atmospheric chloride-induced corrosion of steel-reinforced concrete beam exposed to real marine-environment for 7 years. *Ocean Engineering*, 286, 115675. https://doi.org/10.1016/j.oceaneng.2023.115675

[4]. X. Liu, Z. Yan, D. Wang, R. Zhao, D. Niu, Y. Wang. (2023). Corrosion cracking behavior of reinforced concrete under freeze-thaw cycles. *Journal of Building Engineering*, 64, 105610. https://doi.org/10.1016/j.jobe.2022.105610

[5]. N. Zhao, S. Wang, X. Quan, F. Xu, K. Liu, Y. Liu. (2021). Behavior of polyvinyl alcohol fiber reinforced geopolymer composites under the coupled attack of sulfate and freeze-thaw in a marine environment. *Ocean Engineering*, 238, 109734. https://doi.org/10.1016/j.oceaneng.2021.109734

[6]. R.B. Figueira, R. Sousa, L. Coelho, M. Azenha, J.M. de Almeida, P.A.S. Jorge, C.J.R. Silva. (2019). Alkali-silica reaction in concrete: Mechanisms, mitigation and test methods. *Construction and Building Materials*, 222, 903-931. https://doi.org/10.1016/j.conbuildmat.2019.07.230

[7]. R.-x. Peng, W.-l. Qiu, F. Teng. (2022). Research on performance degradation analysis method of offshore concrete piers in cold regions. *Ocean Engineering*, 263, 112304. https://doi.org/10.1016/j.oceaneng.2022.112304

[8]. Z. He, C. He, X. Kang, X. Huang, S. Wang. (2023). Assessment of structural performance of super large cross-section subsea RC shield tunnels: Emphasis on the combined effects of highly hydrostatic pressure and corrosion-induced deterioration. *Ocean Engineering*, 288, 116134. https://doi.org/10.1016/j.oceaneng.2023.116134

[9]. O. Sengul, M.A. Tasdemir. (2009). Compressive strength and rapid chloride permeability of concretes with ground fly ash and slag. *Journal of Materials in Civil Engineering,* 21(9), 494-501. https://doi.org/10.1061/(ASCE)0899-1561(2009)21:9(494)

[10]. J. Fan, H. Zhu, J. Shi, Z. Li, S. Yang. (2020). Influence of slag content on the bond strength, chloride penetration resistance, and interface phase evolution of concrete repaired with alkali activated slag/fly ash. *Construction and Building Materials*, 263, 120639. https://doi.org/10.1016/j.conbuildmat.2020.120639

[11]. J.W. Visagie, G.M. Moelich, D.M. Meyer, S.S. Kanyenze, M. Kayondo, W.P. Boshoff, R. Combrinck. (2023). Effect of surface curing timing on plastic shrinkage cracking of concrete. *Innovative Infrastructure Solutions*, 8, 61. https://doi.org/10.1007/s41062-022-01032-2

[12]. M. Otieno, H. Beushausen, M. Alexander. (2014). Effect of chemical composition of slag on chloride penetration resistance of concrete. *Cement and Concrete Composites*, 46, 56-64. https://doi.org/10.1016/j.cemconcomp.2013.11

.003

[13]. H. Yildirim, T. Ilica, O. Sengul. (2011). Effect of cement type on the resistance of concrete against chloride penetration. *Construction and Building Materials*, 25(3), 1282-1288. https://doi.org/10.1016/j.conbuildmat.2010.09.023

[14]. J.R.H. Junior, C.E.T. Balestra, R.A. Medeiros-Junior. (2021). Comparison of test methods to determine resistance to chloride penetration in concrete: Sensitivity to the effect of fly ash. *Construction and Building Materials*, 277, 122265. https://doi.org/10.1016/j.conbuildmat.2021.122265

[15]. H.P. Nam, A. Hosoda. (2015). Improvement of water and chloride penetration resistance of slag concrete by using high alite cement. *Proceedings of the JCI*, 37(1), 661-666.

[16]. J. Bao, S. Li, P. Zhang, X. Ding, S. Xue, Y. Cui, T. Zhao. (2020). Influence of the incorporation of recycled coarse aggregate on water absorption and chloride penetration into concrete. *Construction and Building Materials*, 239, 117845. https://doi.org/10.1016/j.conbuildmat.2019.117845

[17]. N.P. Juan, V.N. Valdecantos. (2022). Review of the application of Artificial Neural Networks in ocean engineering. *Ocean Engineering*, 259, 111947. https://doi.org/10.1016/j.oceaneng.2022.111947

[18]. H.-T. Thai. (2022). Machine learning for structural engineering: A state-of-the-art review. *Structures*, 38, 448-491. https://doi.org/10.1016/j.istruc.2022.02.003

[19]. A. Kaveh. (2024). Applications of Artificial Neural Networks and Machine Learning in Civil Engineering. *Studies in Computational Intelligence*. *Springer.* https://doi.org/10.1007/978-3-031-66051-1

[20]. K. Cheng, Z. Lu, C. Ling, S. Zhou. (2020). Surrogate-assisted global sensitivity analysis: an overview. *Structural and Multidisciplinary Optimization*, 61, 1187-1213. https://doi.org/10.1007/s00158-019-02413-5

[21]. E. Borgonovo, E. Plischke. (2016). Sensitivity analysis: A review of recent advances. *European Journal of Operational Research*, 248(3), 869-887. https://doi.org/10.1016/j.ejor.2015.06.032

[22]. A. Kaveh, V.R. Mahdavi. (2018). Optimal domain decomposition using the global sensitivity analysis-based metaheuristic algorithm. *Scientia Iranica*, 25(5), 2480-2487. https://doi.org/10.24200/sci.2017.4508

[23]. A. Kaveh. (2021). Global sensitivity analysis-based optimization algorithm. *Advances in Metaheuristic Algorithms for Optimal Design of Structures, pp. 443-466. Springer*. https://doi.org/10.1007/978-3-030-59392-6_14

[24]. M.M. Moein, A. Saradar, K. Rahmati, S.H.G. Mousavinejad, J. Bristow, V. Aramali, M. Karakouzian. (2023). Predictive models for concrete properties using machine learning and deep learning approaches: A review. *Journal of Building Engineering*, 63, 105444. https://doi.org/10.1016/j.jobe.2022.105444

[25]. A. Kaveh. (2024). The Use of Artificial Neural Networks and Metaheuristic Algorithms to Optimize the Compressive Strength of Concrete. Applications of Artificial Neural Networks and Machine Learning in Civil Engineering, pp. 75-83. *Springer*. https://doi.org/10.1007/978-3-031-66051-1_3

[26]. T. Thilagashanthi, K. Gunasekaran, K.S. Satyanarayanan. (2023). Assessment of chloride ion penetrability and compressive strength prediction in concrete with treated coconut shell aggregates using experimental and ANN approaches. *Asian Journal of Civil Engineering*, 24, 3641-3652. https://doi.org/10.1007/s42107-023-00740-z

[27]. A. Nazari, S. Riahi. (2012). Computer-aided prediction of the ZrO_2 nanoparticles' effects on tensile strength and percentage of water

absorption of concrete specimens. *Journal of Materials Science & Technology,* 28, 83-96. https://doi.org/10.1016/S1005-0302(12)60027-9

[28]. C. Kina, K. Turk, H. Tanyildizi. (2022). Deep learning and machine learning-based prediction of capillary water absorption of hybrid fiber reinforced self-compacting concrete. *Structural Concrete*, 23(5), 3331-3358. https://doi.org/10.1002/suco.202100756

[29]. M. Szafraniec, Z. Omiotek, D. Barnat-Hunek. (2023). Water absorption prediction of nanopolymer hydrophobized concrete surface using texture analysis and machine learning algorithms. *Construction and Building Materials*, 375, 130969. https://doi.org/10.1016/j.conbuildmat.2023.130969

[30]. R.K. Tipu, V. Batra, Suman, V.R. Panchal, K.S. Pandya. (2024). Predictive modelling of surface chloride concentration in marine concrete structures: a comparative analysis of machine learning approaches. *Asian Journal of Civil Engineering*, 25, 1443-1465. https://doi.org/10.1007/s42107-023-00854-4

[31]. J. Castro, D. Bentz, J. Weiss. (2011). Effect of sample conditioning on the water absorption of concrete. *Cement and Concrete Composites*, 33(8), 805-813. https://doi.org/10.1016/j.cemconcomp.2011.05.007

[32]. ASTM International. (2012). ASTM-C140-11a. Standard Test Methods for Sampling and Testing Concrete Masonry Units and Related Units. ASTM, USA. https://doi.org/10.1520/C0140-11A

[33]. JSCE. (2010). JSCE-G572. Test method for apparent diffusion coefficient of chloride ion in concrete by submergence in salt water.

[34]. ASTM. (2004). ASTM C1585-04. Test Method for Measurement of Rate of Absorption of Water by Hydraulic-Cement Concretes.

[35]. J. Zhong, L. Feng, Y.-S. Ong. (2017). Gene expression programming: A survey. *IEEE Computational Intelligence Magazine*, 12(3), 54-72. doi: 10.1109/MCI.2017.2708618

[36]. V.-N. Pham, E. Oh, D.E.L. Ong. (2022). Effects of binder types and other significant variables on the unconfined compressive strength of chemical-stabilized clayey soil using gene-expression programming. *Neural Computing and Applications*, 34, 9103-9121. https://doi.org/10.1007/s00521-022-06931-0

[37]. M.H. Nguyen, V.N. Pham, H.N. Phan, V.H. Do, P.N. Huynh, T.T.T. Mai. (2025). Gene-expression programming-based models for comprehensive evaluation of bond strength and critical slip of various types of FRP bars in concrete. *Structural Concrete*, 26(3), 3700-3719. https://doi.org/10.1002/suco.202301008

[38]. A. Alaskar, G. Alfalah, F. Althoey, M.A. Abuhussain, M.F. Javed, A.F. Deifalla, N.A. Ghamry. (2023). Comparative Study of Genetic Programming-Based Algorithms for Predicting the Compressive Strength of Concrete at Elevated Temperature. *Case Studies in Construction Materials*, 18, e02199. https://doi.org/10.1016/j.cscm.2023.e02199

[39]. A.A. Shahmansouri, H.A. Bengar, S. Ghanbari. (2020). Compressive strength prediction of eco-efficient GGBS-based geopolymer concrete using GEP method. *Journal of Building Engineering*, 31, 101326. https://doi.org/10.1016/j.jobe.2020.101326

[40]. G. Prokopski, J. Halbiniak. (2000). Interfacial transition zone in cementitious materials. *Cement and Concrete Research*, 30(4), 579-583. https://doi.org/10.1016/S0008-8846(00)00210-6

[41]. K. Lyu, E.J. Garboczi, W. She, C. Miao. (2019). The effect of rough vs. smooth aggregate surfaces on the characteristics of the interfacial transition zone. *Cement and Concrete Composites*, 99, 49-61. https://doi.org/10.1016/j.cemconcomp.2019.03.001